Experimental Techniques (2021) 45:287–296
https://doi.org/10.1007/s40799-020-00393-6

S.I. : COMPUTER VISION AND SCANNING LASER VIBROMETRY METHODS

Modal Parameter Estimation of a Compliant Panel Using Phase-based Motion Magnification and Stereoscopic Digital Image Correlation

M. Eitner[1] · M. Musta[1] · L. Vanstone[1] · J. Sirohi[1] · N. Clemens[1]

Received: 19 April 2020 / Accepted: 4 August 2020 / Published online: 24 August 2020

Abstract

This paper demonstrates the use of broad-band phase based motion magnification (PMM) to improve the modal parameter estimation from high-speed stereoscopic digital image correlation (DIC). PMM is used as a diagnostic technique to investigate the free vibration response of a panel. The compliant panel, consisting of a thin polycarbonate sheet, forms a test section wall in a supersonic blow-down wind tunnel, where it is used to investigate supersonic fluid-structure interaction in the presence of shock wave boundary layer interaction. The panel is excited by an impact hammer and the transient deformation is captured using high-speed cameras. The original and motion-magnified images are input to a digital image correlation algorithm to calculate the out-of-plane deformation of the panel. The measured deformation is used to extract the modal parameters of the compliant panel. By using PMM as a preprocessing tool in a broad frequency band containing multiple structural modes, the signal to noise ratio of the measured deformation is improved. The use of PMM improves the estimated mode shapes, increasing the MAC value of the first mode compared to FEM predictions from 0.29 to 0.99. Motion magnification also improves the coherence between measured input force and panel deformation by up to 13% if suitable parameters are chosen.

Keywords Modal analysis · Phase-based motion magnification · Digital image correlation · Impact testing · Fluid-structure interaction

Introduction

The analysis of fluid-structure interaction (FSI) in supersonic flow is of increasing importance in the context of supersonic vehicle design, where shock waves impinging on lightweight structures can lead to large aero-thermal and structural loads, potentially leading to destructive instabilities. Computational modeling of shock wave boundary layer interactions is very expensive due to the unsteadiness and highly coupled nature of these processes [1]. Therefore in recent years, several researchers have investigated supersonic panel FSI experimentally, using high-speed optical methods to measure the deformation of compliant panels with impinging shocks, see for example [2, 3]. Especially the use of high-speed stereoscopic DIC has been well established in this community to record the full-field structural responses [4, 5].

The present work is part of a larger project that investigates the FSI induced by shock-induced separation over a compliant panel in supersonic flow. Experiments were performed in a Mach 2 wind tunnel in which one part of the test section was replaced by a thin polycarbonate panel placed upstream of a 20° compression ramp. The shock and separated flow induced by the ramp are unsteady and result in transient deformation of the panel, which in turn affects the flow field and shock motion. The panel deformation was optically measured using Digital Image Correlation (DIC), by painting a speckle pattern on the outside of the panel and imaging it with two high-speed cameras. This method allows measurement of the panel deformation without affecting structural or mass properties even in the presence of high-speed flow.

In order to understand the dynamic behavior of the panel under these complex flow conditions, the first step is to characterize its free vibration properties. To this end, a finite

✉ M. Eitner
marceitner@utexas.edu

[1] Department of Aerospace Engineering and Engineering Mechanics, The University of Texas at Austin, Austin, TX, USA

element model (FEM) of the panel was constructed and validated experimentally. An impact hammer was used to excite the panel by striking the wall of the wind tunnel adjacent to the panel. The panel response (out-of-plane deformation) to the impact was measured using high-speed stereoscopic digital image correlation (DIC) and the modal properties of the panel were estimated using the Complexity Pursuit (CP) approach.

An issue with the displacement data obtained from high-speed DIC is its potentially low signal to noise ratio (SNR), especially at higher frequencies. This is usually the limiting factor for the identification of higher structural modes. A technique that has recently been introduced in the modal analysis community involves the use of phase-based motion magnification (PMM) to increase the SNR of displacement data obtained from high-speed images. PMM is a video processing technique that allows the magnification of sub-pixel motion in a pre-defined frequency band [6]. Through the use of spatial and temporal filters, local motion in a video can be magnified, with minimal noise magnification, thus resulting in a reconstructed video that exhibits larger SNR [7]. When DIC or point tracking algorithms are used on these motion-magnified videos, the resulting deformation data can be more accurate.

PMM can therefore be used as a preprocessor to the DIC algorithm. This can be done in two ways. The first is to pick a structural mode, whose resonant frequency has been approximately identified, and then magnify the motion only in a narrow frequency band centered around that mode. The magnified video then shows the mode shape/operational deflection shape of the structure. This process has been successfully used in combination with DIC in both two-dimensional and three-dimensional applications [8–11]. This process has also successfully been applied to numerically simulated stereoscopic images [12]. The second way is to magnify the motion in a broad frequency band, including multiple modes of interest. In a previous study [13], high-speed images of a reduced-scale rocket nozzle under operating conditions were magnified in a frequency band containing the first six modes. That specific study used images from a single camera and performed point tracking to measure the structural deformations. The present work can be seen as the natural extension of that method to stereoscopic DIC.

In the present study, out-of-plane panel deformation is measured using DIC as well as broad-band motion-magnified images input to DIC (called PMM-DIC). These two sets of deformation data are input to a modal estimation algorithm and the effect of motion-magnification on the estimated modal parameters is quantified. Section two of this paper outlines the full modal parameter estimation process used, including details about the DIC setup as well as details about the PMM algorithm. In section three the effect of PMM on output-only modal parameter estimation is discussed. Section four investigates the effect that the preprocessing with PMM has on the coherence between input force and output deformation.

Experimental Setup and Methods

This section offers an overview of the experimental setup and methodology used to perform the deformation measurement and modal parameter estimation. Relevant theory and information about each measurement and data processing step are discussed.

Figure 1 shows an outline of the modal parameter estimation process. The first step is the experimental portion, where a structure is excited through a force from an impact or shaker or flow-induced pressure field. In the present case, the structure (the panel) was excited by an impact hammer strike. The resulting deformation was recorded using high-speed cameras. The deformation can either directly be extracted using DIC (top path in Fig. 1), or the images can be first motion-magnified using the PMM algorithm and then processed by DIC (bottom path in Fig. 1). In both cases, the out-of-plane deformation of the panel is eventually obtained and modal analysis can be performed.

In addition, a finite element model of the compliant panel was generated to provide numerical predictions of the natural frequencies and mode shapes; these were used to check the validity of the experimentally derived modal parameters.

Test Articles and Input Forcing

Figure 2(a) shows the test section of the wind tunnel with the compliant panel located upstream of a shock-inducing compression ramp. A schematic of the full experimental setup is shown in Fig. 2(b). The cross-sectional area of the test section is approximately 20 cm × 15 cm.

The compliant panel is made of polycarbonate (Young's modulus 2.6 GPa) of length 127 mm and width 68.5 mm.

The panel was designed to exhibit low natural frequencies to fall in the range of known flow unsteadiness. Due to the constraints of the wind tunnel test section size, the panel could not be manufactured from steel and still exhibit low natural frequencies. Thus, a soft material such as polycarbonate (PC) was chosen instead. The panel insert is machined from a block of PC, from which a pocket is cut out until the desired thickness is achieved. The insert is fixed to the wind tunnel floor through ten bolts and sealed with an O-ring. A model of the panel insert is shown in Fig. 3(a).

An impact hammer (modally tuned PCB hammer) with a steel tip was used to deliver an impulsive force to the wind

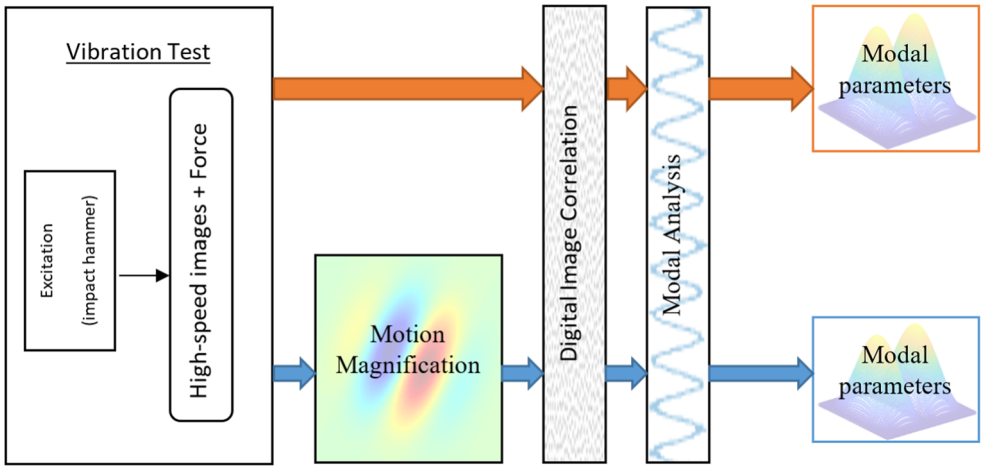

Fig. 1 Outline of the modal parameter estimation process

tunnel wall, near a corner of the compliant panel (indicated by yellow tape in Fig. 2(a)). Since the panel is flexible, direct impact of the panel resulted in a low bandwidth excitation spectrum; not more than the lowest 200 Hz could be properly excited in this way. By impacting the steel wind tunnel wall instead, a uniform force spectrum from 0 Hz - 1500 Hz was achieved. Two compliant panels of thickness 1.0 mm and 1.5 mm were tested, each subjected to multiple impacts.

The applied load was measured by a load cell in the impulse hammer and recorded at 4 kHz. At the same time, the resulting transient deformation of the panel was recorded by the high-speed cameras. The data was then used to analyze the effect of PMM on output only modal analysis (see "Effect of PMM on Output-only Modal Parameter Estimation") and on coherence (see "Effect of PMM on Coherence").

Digital Image Correlation (DIC)

High-speed stereoscopic DIC was used to measure the transient deformation of the compliant panel. The lower side of the panel from the point of view of one of the two cameras is shown in Fig. 3(b). The speckle pattern was drawn manually on the panel with a small black marker. Two Phantom Miro M310 cameras were used to record the images for DIC at a frame rate of 4 kHz with an image size of 832 × 448 px and a resulting resolution of 6.0 px/mm; images were captured for approximately one second after the impulsive excitation. The cameras were placed approximately 1 m apart at a distance of about 67 cm below the compliant panel. Note that this rather large stereo angle was necessary due to the position of the LED light sources directly under the panel. The panel was illuminated using two LED lights placed directly under the panel. The commercial software Davis10 (by Lavision Inc.) was used for DIC processing. A flat calibration plate with evenly spaced markers was used during the calibration process, and reference images were taken at out-of-plane offsets of $\pm 1mm$ from the origin position. The calibration resulted in a third order polynomial fitting function with an average rms error of less than 0.5 px. An interrogation window size of 15×15 px was chosen and the distance between neighboring interrogation windows was set to 5 px. This resulted in a deformation grid of 66 × 116 discrete points on the panel. Since the grid changes slightly from frame to frame, the

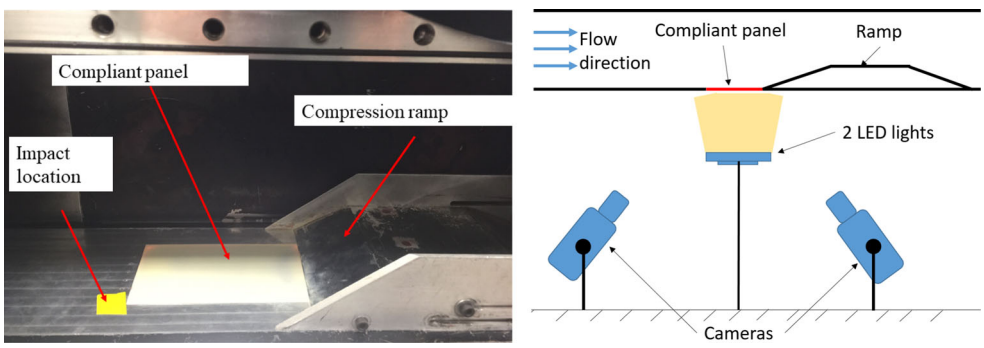

(a) (b)

Fig. 2 **a** photograph of the compliant panel and compression ramp mounted in the wind tunnel, and **b** schematic diagram of the DIC setup

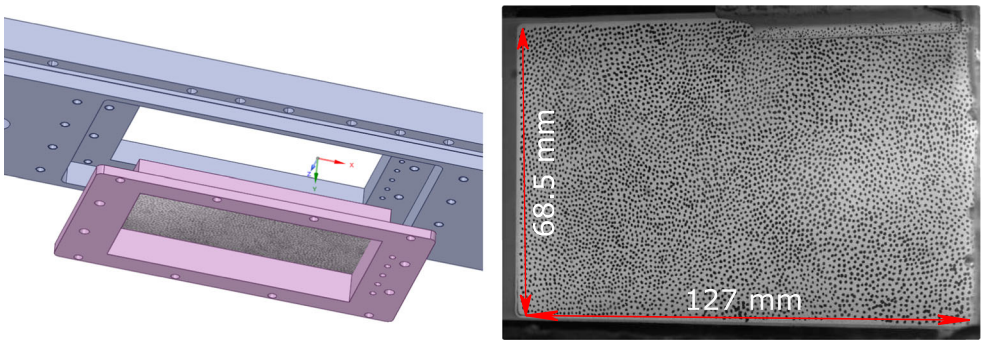

(a) (b)

Fig. 3 Panel insert and DIC speckle pattern, viewed from below the wind tunnel

data was then interpolated to obtain the deformation at a fixed grid location, resulting in a final deformation grid containing approximately 5700 degrees of freedom.

Phase-based Motion Magnification (PMM)

The phase-based motion magnification algorithm by Wadhwa et al. [6] was used in this work. The algorithm performs the motion magnification in several steps:

1. Each image in the video is first subjected to a two-dimensional Fourier transform, resulting in real and imaginary components.
2. Next, 98 scales of each image are created, varying in resolution. For each image in this new set, a group of oriented Gabor filters is created, which allows the extraction of localized motion. This process is based on the Complex Steerable Pyramid Decomposition developed by Simoncelli et al. [14]. The so-called 'half octave' configuration is chosen which employs a total of 82 spatial filters distributed among 8 angular orientations. This specific configuration yields good magnification results while also being computationally compact, see [6] for more details.
3. This process of decomposition and spatial filtering is repeated for each image in the video.
4. The imaginary part of each decomposed and filtered image is now subtracted from that of the very first image in the video. Therefore all phase information (contained in the imaginary part) is relative to the first image.
5. A magnification factor α is then multiplied with the imaginary part of the decomposed and filtered image sets. Since the motion in a video is primarily contained in the phase information, this multiplication factor has the effect of actually magnifying the local motion in the video.
6. Finally, the sets of images are collapsed to result in a single motion-magnified image for each frame of the video.

The motion-magnified images of the deforming speckle pattern are then input to the DIC software for the PMM-DIC measurement procedure.

Modal Analysis

The modal parameters of the panel are estimated from the out-of-plane deformation of the panel resulting from the impact hammer strike measured using DIC and PMM-DIC. Although the applied impulse was measured in this test, an output-only modal analysis algorithm was chosen to enable extraction of modal parameters in future tests involving unknown excitation from the internal supersonic flow. The Complexity Pursuit (CP) algorithm [15] was chosen for this task. The CP algorithm assumes that its input $[x]$, a set of simultaneous temporal measurements, is a linear mixture of less complex 'source signals' $[s]$. The algorithm then outputs estimates of these 'source signals' as well as the linear mixing matrix $[A]$ of the measured system:

$$[x] = [A][s] \tag{1}$$

Although CP was originally developed for speech processing, the structural dynamics community has found it to be a useful tool for output-only modal analysis [16, 17]. From a structural point of view, the dynamic response of a system can be expressed as a linear combination of mode shapes and modal coordinates. When the input to the CP algorithm, $[x]$ is structural deformation data, the estimated 'source signals' $[s]$ are the modal coordinates of the system, and the mixing matrix $[A]$ is the modal matrix. In the present work, the inputs to the CP algorithm are the out-of-plane displacement time histories of each point extracted with DIC or PMM-DIC. The outputs are the modal matrix as well as the modal coordinates, from which natural frequencies and damping ratios can be estimated by curve-fitting.

Model Reduction Through Singular Value Decomposition (SVD)

The CP algorithm outputs the same number of natural frequencies and mode shapes as the number of degrees of freedom. If the number of displacement measurement points is m (in the present case $m \sim 5700$), at each of n steps in the time history (in the present case, $n \sim 4000$), this will lead

to a large data set and a high computational burden. Note that only the first few modes of the panel participate in the response, therefore the remainder of the identified modes are spurious modes. Hence it is more efficient to retain a small subset of the input degrees of freedom for processing by the CP algorithm.

From the measured displacement time histories, the number of degrees of freedom is reduced using Singular Value Decomposition (SVD). Yang et al. [18] demonstrated good results using a combination of CP and SVD; the same procedure was followed in this work. The first step in this process is to compute the SVD of the measurement matrix $[X]$ (size $m \times n$) as:

$$[X] = [U][S][V]^T \tag{2}$$

The true dimensionality of the system can be estimated by examining the singular values contained in the main diagonal of the matrix $[S]$ (size $m \times n$). Most information of the system dynamics will be contained in only a few modes, corresponding to the largest singular values. The system degrees of freedom can then be reduced by choosing the largest r singular values.

The measurement matrix of the reduced system is computed as:

$$[X_r] = [U_r]^T [X] \tag{3}$$

where $[U_r]$ (size $m \times r$) consists of the first r columns of the matrix $[U]$ (size $m \times m$) from the SVD. The reduced measurement matrix $[X_r]$ (size $r \times n$) is then used as an input to the CP algorithm to estimate the modal parameters. In a final step, each estimated modal vector of this reduced system $[\gamma]$ (size $r \times 1$) needs to be multiplied by $[U_r]$ to obtain the modal vector of the full system $[\Phi]$ (size $m \times 1$):

$$[\Phi] = [U_r][\gamma]. \tag{4}$$

In addition to reducing the computational cost, the model reduction also greatly facilitates the modal analysis by reducing the number of spurious modes. Since the CP algorithm outputs as many modes as channels in the input signal, it remains the user's task to sort through all resulting modes and separate physical from spurious ones. If only a low number of r modes are estimated from the reduced system, this task becomes much easier.

Finite Element Model (FEM)

A finite element model of each panel was constructed in ANSYS and modal analysis was performed. The panel was constructed using four-node shell elements, clamped boundary conditions were applied and mesh convergence was achieved. The FEM model was slightly modified by varying the thickness of the panel by several micrometers such that the lowest natural frequency matches closely with that obtained from the experiments. The first three mode shapes and natural frequencies of the 1.5 mm thick panel predicted by the FEM model are shown in Fig. 4. The mode shapes for the 1.0 mm panel were similar to that of the thicker panel, and its first three natural frequencies were f_1 = 407 Hz, f_2 = 542 Hz, f_3 = 799 Hz.

Results and Discussion

A preliminary validation case was performed to demonstrate the validity of the PMM method. A piezo-electric actuator was bonded to the center of the panel. A thin copper shim was used as an anode. The setup is shown in Fig. 5(a). During the bonding process the initially painted speckle pattern was smeared and had to be redrawn. A can of spray paint was used to cover the panel including the piezo actuator in white paint and black speckles were then drawn with a pen. The panel was then installed in the wind-tunnel and excited by a 400 Hz sinusoidal signal from a high-voltage piezo amplifier. The resulting bending moment induced in the panel led to out-of plane oscillations with an amplitude of up to $13\mu m$. The deformation was recorded for one second at 2 kHz and the out-of-plane deformation was then computed with the DIC software. The images were then motion magnified from 300 to 700 Hz by a factor of 3 and once again the out-of-plane deformation was computed with the DIC software. The power spectra extracted with both methods are shown in

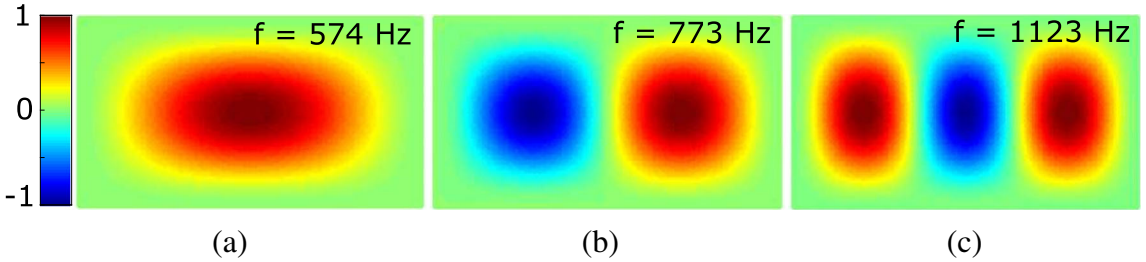

Fig. 4 Mode shapes and natural frequencies of **a** first, **b** second and **c** third mode as predicted by the Finite Element Model (1.5 mm thick panel)

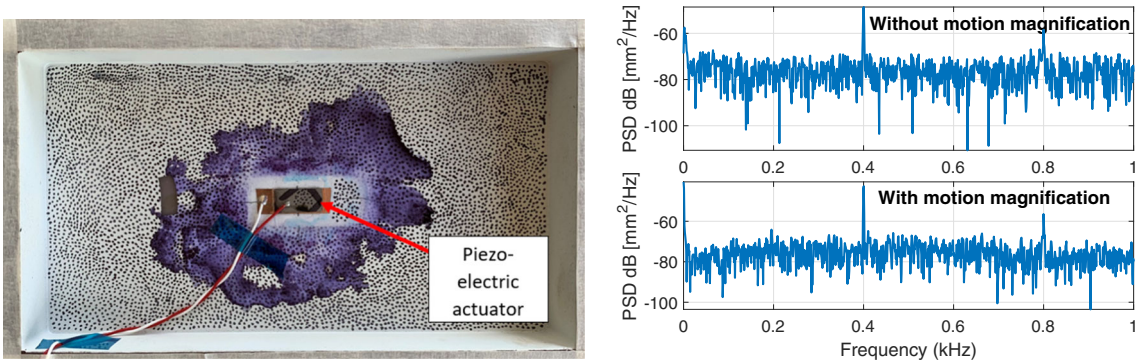

Fig. 5 Validation case. **a** Piezo-electric actuator attached to panel and **b** resulting power spectra from DIC at same location

Fig. 5(b). Both methods correctly identify the dominant frequency at 400 Hz.

A typical impulse response of the mid-point of the 1.5 mm thick panel along with the measured impact force are shown in Fig. 6(a). The peak displacement of the panel is less than 30 μm. Such a small value is expected since the panel is not impacted directly, but rather subjected to the base motion excitation of the wind tunnel. As expected for polymer materials, the polycarbonate panel exhibits relatively large damping and the system response drops to the noise floor within the first 0.1 seconds of the impact. The power spectrum of the same impulse response is shown in Fig. 6(b).

Preliminary analysis of the panel using the FEM model indicated that the fundamental frequency was approximately 570 Hz, thus a 9^{th} order Butterworth bandpass filter (500 − 1990 Hz) was chosen to filter the displacement measured using DIC as well as PMM-DIC. Note that the displacement data shown in Fig. 6 has already been bandpass filtered. A peak is observed in the power spectral density around 570 Hz corresponding to the first mode, while the peak corresponding to the third mode is not so evident. Note that there is no contribution of the second mode to the displacement at the mid-point of the panel since this location is a node.

Model Reduction

The plot of the singular values for the displacement obtained with DIC (without PMM) is shown in Fig. 7 in descending order. It can be seen that there is a steep decrease in magnitude over the first four singular values, after which the singular values gradually approach zero. Several values for the number of reduced singular values were tested with minimal effect on the resulting modal parameters. All results in the following discussion were obtained with the highest 12 singular values, i.e., $r = 12$, for the reduced model.

Effect of PMM on Output-only Modal Parameter Estimation

The power spectra from the original (DIC) and 3x motion-magnified (PMM-DIC) displacements at two different locations on the 1.5 mm thick panel are shown in Fig. 8. The two locations are indicated by the position of the red

Fig. 6 Deformation of the mid-point of the panel and impact force vs. time (no motion magnification). Response has been bandpass filtered from 500-1990 Hz

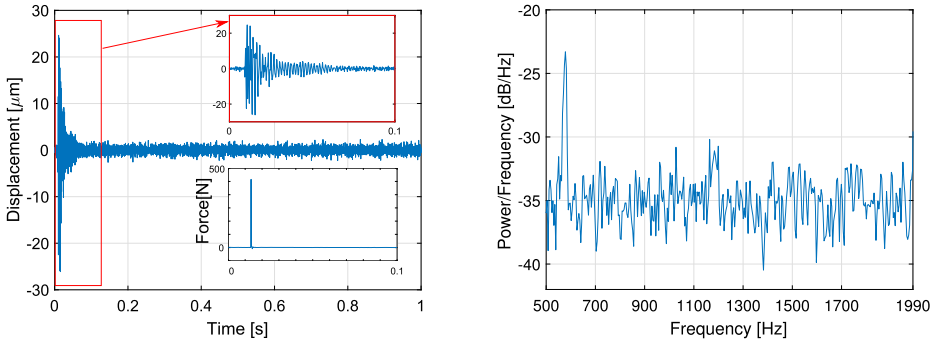

(a) Time history of panel displacement and input force. (b) Power spectral density of panel displacement

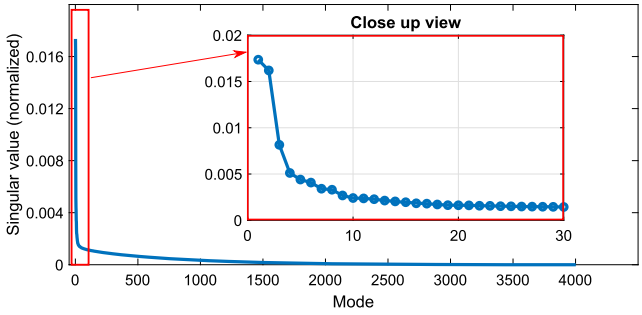

Fig. 7 Distribution of singular values of measurement matrix

dot in the inset of the plots; location (**A**) is at the mid-point of the plate while location (**B**) is on the mid-line, approximately 39 mm towards one end of the plate. The main difference between the original displacement and the motion-magnified displacement can be seen in the peak corresponding to the first mode at around 570 Hz. Motion magnification appears to significantly improve the signal to noise ratio at this mode, especially at location **B** towards one end of the plate. Note that the displacement due to the first mode is maximum at the mid-point of the plate (location **A**) and is much less at location **B**. Therefore, the motion magnification has the greatest effect for the first mode at location **B**.

The results of the modal parameter estimation are shown in Fig. 9. The power spectra of the separated modal coordinates show only one significant peak, indicating that the CP algorithm worked successfully. Contour plots of the mode shapes (in terms of the out-of-plane deformations) are shown for the first three modes along with the modal assurance criterion (MAC), which compares each mode with the corresponding mode from the FE model. It can be seen that PMM-DIC leads to an overall improvement of MAC values, especially in the case of the first mode. This improvement in the first mode shape estimate is consistent with the improvement of SNR seen in the power spectra (Fig. 8).

Considering the large improvement in the first mode shape, further investigation has been performed. After the system is reduced to the 12 most energetic SVD modes, the first two SVD modes looks very similar for both cases, as can be seen in Fig. 10. The energetic order of the first two modes however is switched. After Blind Source Separation is applied to the first SVD 12 modes of the reduced system, significant differences appear especially between the first separated normal mode of the motion magnified images and the non-magnified ones. It seems that the BSS algorithm exhibits a strong sensitivity to its input, which is somehow exploited by use of the motion magnification. Further investigations into this relationship are needed.

Note that there seems to be a small peak in the power spectrum of the first modal coordinate in the motion magnified case at around 500 Hz (Fig. 8(b)), not present in the original modal coordinate. The reason for this spurious mode is unclear and further investigation into its origin is the goal of future work.

Effect of PMM on Coherence

The previous section discussed the effect of motion magnification on the mode shapes estimated using an output-only analysis. The quality of the estimated modes was determined by using the MAC to compare the experimentally determined mode shapes with those predicted by the FEM model. Another parameter that can be used to assess the effect of motion magnification is the coherence between the input forcing and the response. Using the measured input impulse, the magnitude squared coherence function η can be readily calculated as

$$\eta(\omega) = \frac{|S_{xf}(\omega)|^2}{S_{xx}(\omega)S_{ff}(\omega)} \tag{5}$$

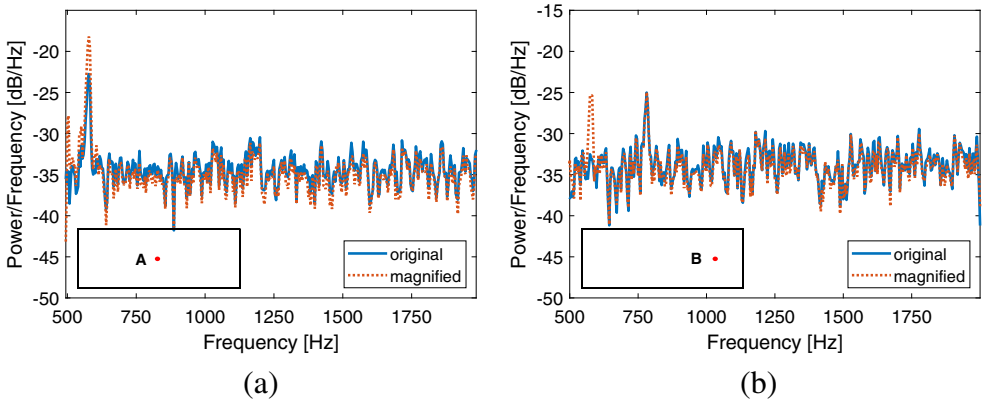

Fig. 8 Comparison of power spectra with and without motion magnification at two different locations on the panel (location on panel shown in bottom left of each figure)

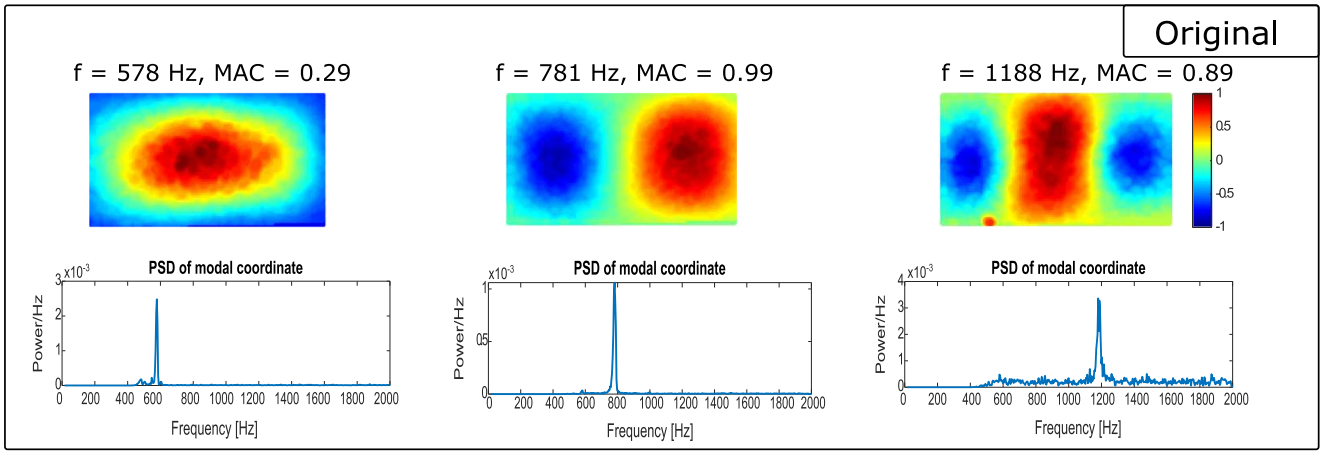

(a)

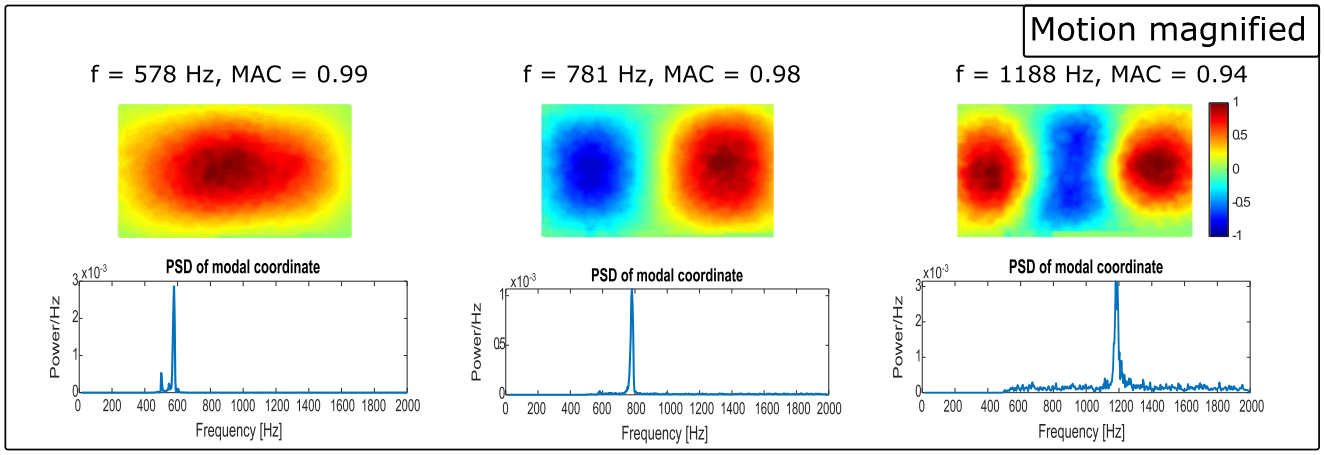

(b)

Fig. 9 Comparison of modal parameter estimation **a** without and **b** with 3x motion magnification

where $S_{xx}(\omega)$ and $S_{ff}(\omega)$ are the auto power spectral density functions of the displacement and input force respectively. $S_{xf}(\omega)$ is the cross power spectral density function between the displacement and the force. Thus, the effect of motion magnification can be quantified by analyzing whether the coherence in the magnified frequency band is improved.

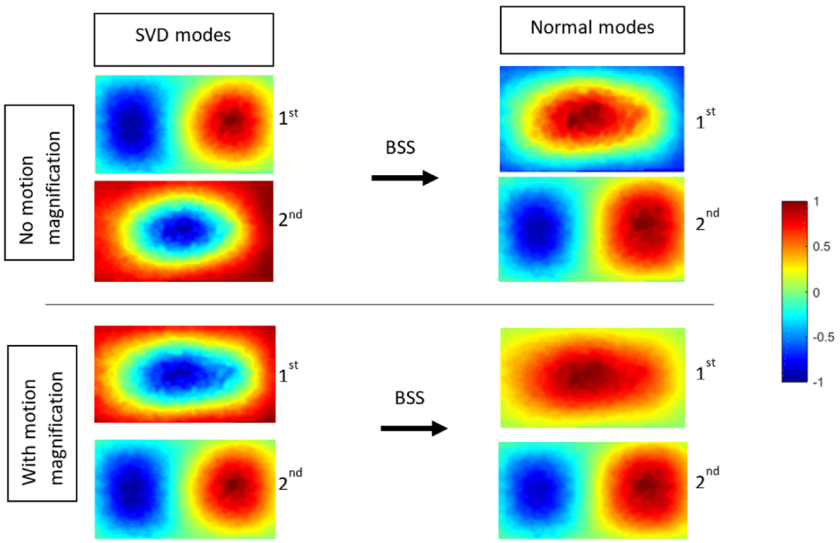

Fig. 10 Difference between SVD modes and normal modes due to motion magnification

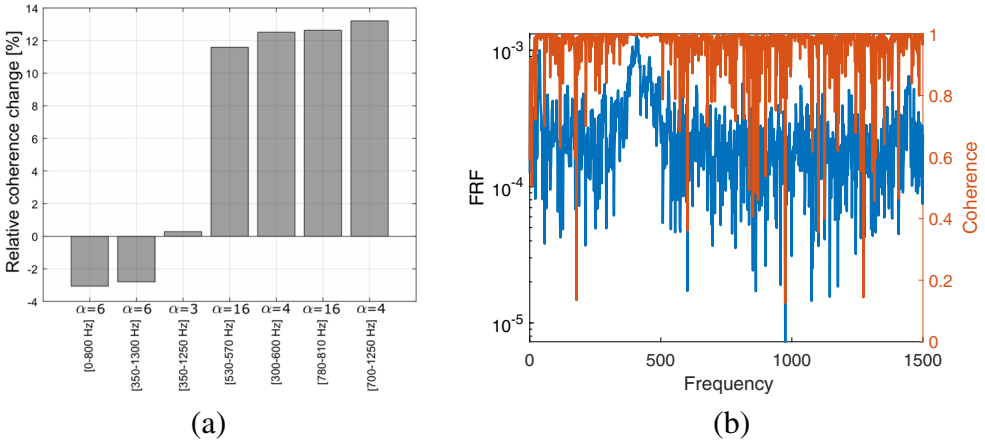

Fig. 11 **a** Relative change of coherence due to motion magnification, from impact data of 1.0 mm thick panel; **b** example of FRF and coherence near panel center

Motion magnification was performed with several combinations of the magnification factor α and the magnified frequency band, and their effect on the coherence was studied. For each impact test, the mean value of the coherence was computed within the chosen frequency band with and without motion magnification. After averaging the results over all impact tests, a 'relative coherence change' Δ_{coh} value is computed as

$$\Delta_{coh} = \frac{\text{mean coherence after PMM} - \text{mean coherence before PMM}}{\text{mean coherence before PMM}} \tag{6}$$

The relative coherence change for seven combinations of magnification factor and frequency band are shown in Fig. 11(a). The first two combinations featuring broad-band motion magnification with a magnification factor of six result in reduced coherence. All the other combinations result in increased coherence; in general it can be concluded that either a small magnification factor or a narrow frequency band must be chosen to improve the coherence values. This trend seems consistent with previous experience, since it is known that large magnification factors can only be used in narrow frequency bands and will otherwise result in unwanted image artifacts and excessive blurriness. A sample of the coherence along with the FRF computed for the non-magnified case is shown in Fig. 11(b).

Summary and Conclusions

A thin polycarbonate panel was excited by a hammer impact and the deformation was recorded with two high-speed cameras. Digital image correlation (DIC) was used to compute the out-of-plane deformation of the panel, using both the original camera images as well as motion-magnified camera images (PMM-DIC). Given the small deformation of the panel ($< 30\mu$m) and resulting low signal-to-noise ratio, the goal of the study was to assess the effectiveness of motion-magnification, i.e., deformation measured using PMM-DIC on the estimated modal characteristics of the panel.

Output-only modal analysis was performed using singular value decomposition model order reduction technique followed by the complexity pursuit (CP) algorithm. The model reduction reduced the processing time for the CP algorithm from 38 minutes to about 30 seconds. The estimated mode shapes were compared to finite element predictions and it was shown that the second and third mode lead to high MAC values, whereas the first mode shape showed low agreement (MAC=0.29). Motion magnification was then applied to the high-speed images in a broad frequency band (500-1990 Hz) containing the first three structural modes. The motion magnified images were then used to perform the same analysis (DIC - model reduction - complexity pursuit). The mode shapes obtained from the PMM-DIC method showed better agreement with the FEM predictions, for example, the MAC value for the first mode increased from 0.29 to 0.99. The estimated natural frequencies were unaffected by motion magnification. By comparing the power spectra of the out-of-plane displacement of the DIC and PMM-DIC method at a single point on the panel, it was shown that the use of PMM led to a clear improvement of SNR in the first mode.

The importance of choosing a good combination of magnification factor and frequency band was shown by computing and comparing the magnitude squared coherence function before and after motion magnification. If a broad frequency band is chosen for motion magnification, the magnification factor must be relatively small (around 3-5) to result in improved coherence values. Coherence could be improved by up to 13% if the right combinations of magnification factor and frequency band were chosen.

In conclusion, the PMM-DIC technique can be used to improve modal parameter estimation for a structure undergoing small amplitude vibration, where the signal to noise ratio of the measurements is low. Future work in this

direction could involve investigation of the role of image blurring on estimated modal parameters. Image blurring is a side effect of PMM and it is known that this can have a positive effect on DIC deformation measurements.

Acknowledgements The authors thank Jeremy Jagodzinski for assistance with the measurements.

Funding Information The work was supported by the National Science Foundation under award #1913587.

Data Availability All data is available.

Compliance with Ethical Standards

Conflict of interests On behalf of all authors, the corresponding author states that there is no conflict of interest.

Code availability Custom Matlab code and DAVIS digital image correlation software.

References

1. Dolling DS (2001) Fifty years of shock-wave/boundary-layer interaction research: What next? AIAA J 39(8):1517–1531. https://doi.org/10.2514/2.1476
2. Neet MC, Austin JM (2020) Effects of surface compliance on shock boundary layer interaction in the caltech mach 4 ludwieg tube. In: AIAA Scitech 2020 forum, pp 0816. https://doi.org/10.2514/6.2020-0816
3. Peltier SJ, Rice BE, Szmodis J, Ogg DR, Hofferth JW, Sellers ME, Harris AJ (2019) Aerodynamic response to a compliant panel in mach 4 flow. In: AIAA Aviation 2019 forum, pp 3541. https://doi.org/10.2514/6.2019-3541
4. Beberniss TJ, Ehrhardt D (2020) Visible light refraction effects on high-speed 3-dimensional digital image correlation measurement of a thin panel in mach 2 flow. In: International modal analysis conference 38
5. Spottswood S, Eason T, Beberniss T (2012) Influence of shock-boundary layer interactions on the dynamic response of a flexible panel. In: ISMA 2012 International conference on noise and vibration engineering. Katholieke Universiteit Leuven Leuven, Belgium, pp 603–617
6. Wadhwa N, Rubenstein M, Fredo D, Freeman WT (2013) Phase-based video motion processing. ACM Trans Graphics 32(4):80:1–80:10. https://doi.org/10.1145/2461912.2461966
7. Fleet DJ, Jepson AD (1990) Computation of component image velocity from local phase information. Int J Comput Vis 5:77–104. https://doi.org/10.1007/BF00056772
8. Harmanci YE, Gülan U, Holzner M, Chatzi E (2019) A novel approach for 3d-structural identification through video recording: magnified tracking. Sensors 19(5):1229. https://doi.org/10.3390/s19051229
9. Molina-viedma ÁJ, López-alba E, Felipe-sesé L, Díaz FA (2019) Operational deflection shape extraction from broadband events of an aircraft component using 3D-DIC, in magnified images. Shock Vib 2019:9. https://doi.org/10.1155/2019/4039862
10. Poozesh P, Sarrafi A, Mao Z, Avitabile P, Niezrecki C (2017) Feasibility of extracting operating shapes using phase-based motion magnification technique and stereo-photogrammetry. J Sound Vib 407:350–366. https://doi.org/10.1016/j.jsv.2017.06.003
11. Sarrafi A, Mao Z (2017) Wind turbine blade damage detection via 3-dimensional phase-based motion estimation. In: The 11th international workshop on structural health monitoring. https://doi.org/10.12783/shm2017/14154
12. Rohe DP (2020) Experimental modal analysis using phase quantities from phase-based motion processing and motion magnification. In: International modal analysis conference 38
13. Eitner MA, Miller BG, Sirohi J, Tinney CE (2019) Operational modal analysis of a thin-walled rocket nozzle using phase-based image processing and complexity pursuit. In: Niezrecki C, Baqersad J, Di Maio D (eds) Rotating machinery, optical methods & scanning LDV methods. Springer International Publishing, pp 19–29. https://doi.org/10.1007/978-3-030-12935-4_3
14. Simoncelli E, Freeman WT (1995) The steerable pyramid: a flexible architecture for multi-scale derivative computation. In: Proceedings of the 1995 international conference on image processing. https://doi.org/10.1109/ICIP.1995.537667
15. Stone JV (2001) Blind source separation using temporal predictability. Neural Comput 13(7):1559–1574. https://doi.org/10.1162/089976601750265009
16. Antoni J, Castiglione R, Garibaldi L (2017) Interpretation and generalization of complexity pursuit for the blind separation of modal contributions. Mech Syst Signal Process 85:773–788. https://doi.org/10.1016/j.ymssp.2016.09.009
17. Eitner MA, Sirohi J, Tinney CE (2019) Modal parameter estimation of a reduced-scale rocket nozzle using blind source separation. Measurement Sci Technol 30(9):095401. https://doi.org/10.1088/1361-6501/ab228f
18. Yang Y, Dorn C, Mancini T, Talken Z, Kenyon G, Farrar C, Mascareñas D (2017) Blind identification of full-field vibration modes from video measurements with phase-based video motion magnification. Mech Syst Signal Process 85:567–590. https://doi.org/10.1016/j.ymssp.2016.08.041